Applied Catalysis B: Environmental 338 (2023) 123002

Contents lists available at ScienceDirect

Applied Catalysis B: Environmental

journal homepage: www.elsevier.com/locate/apcatb

Alkane metathesis over immobilized pincer-ligated iridium complexes: Effect of support nature

Cristina Megías-Sayago [a,*], Ignacio Centeno-Vega [a], Luis F. Bobadilla [b], Svetlana Ivanova [b], Nuria Rendón [a], Andrés Suarez [a]

[a] Departamento de Química Inorgánica, Instituto de Investigaciones Químicas and Centro de Innovación en Química Avanzada (ORFEO-CINQA), Centro Mixto CSIC-Universidad de Sevilla, 41092 Sevilla, Spain
[b] Departamento de Química Inorgánica e Instituto de Ciencia de Materiales de Sevilla, Centro Mixto CSIC-Universidad de Sevilla, 41092 Sevilla, Spain

ARTICLE INFO

Keywords:
Alkane metathesis
Immobilized complex
Iridium complex
Plastic upcycling approach
Support effect

ABSTRACT

In this work, catalytic alkane metathesis has been evaluated as a suitable approach to upcycle hydrocarbons (polyolefins) at moderate temperatures. To this end, a pincer-ligated iridium complex (dehydrogenation catalyst) has been combined with a rhenium-based (metathesis) catalyst, being the effect of immobilizing the Ir complex over different supports deeply investigated. FTIR spectroscopy has been used to confirm the complex grafting and to elucidate the anchoring site to the support. Additionally, the supports have been dehydroxylated at different conditions to evaluate its possible impact in both the complex grafting and the catalytic activity. The influence of the support nature and its participation in the catalytic reaction have been clearly evidenced.

1. Introduction

Imagining a world without the presence of synthetic plastics is almost impossible due to the essential role they play in every aspect of modern life. Plastics have been linked to most impactful advancements of society in the last decades, highly improving humans' life quality. Among them, polyolefins constitute 65 % of global polymer production [1] being polyethylene and polypropylene (PE and PP, respectively) the largest-volume synthetic polymers [2]. The latter is a direct consequence of its chemical robustness, high mechanical strength, thermal stability and, logically, of its low cost [3].

These hydrocarbon-based polymers are extremely inert which makes its degradation by low-energy chemical processes a challenging problem. There is no simple way to transform them selectively into useful products, especially at moderate temperatures [1,4,5]. This results in a major environmental concern, since most plastics are accumulated in landfills or environment, where they may take centuries to degrade and disappear naturally. In addition to this, the increasing need for a larger plastic production along with the depletion of petroleum supplies over the last decades, generates a rising interest in studying diverse methods for obtaining fuels and chemicals from other carbon feedstocks.

Among the different approaches to upcycle polyolefins at moderate temperatures, catalytic hydrogenolysis stands up as technology that cleaves polyolefins' C-C bonds to form lighter hydrocarbons that can be used as fuels and/or chemical feedstocks [6–8]. Unfortunately, the need of large amounts of co-reactant, *i.e.* hydrogen, forces somehow the pursuit of alternatives [6].

In this context, catalytic alkane metathesis emerges as an appropriate option to convert hydrocarbons at moderate temperatures [9–11]. This process entails the use of a tandem catalyst which usually consists of a combination of two independent functions: one active in the alkane dehydrogenation reaction and other in the alkene metathesis process [9,10], which is usually based on Re_2O_7. Both systems are needed to complete the catalytic cycle, which can involve one alkane [12] or a mixture of them [10]. The latter, known as cross-alkane metathesis (CAM) process, occurs *via* C–H activation of two different alkanes, one being lighter.

The CAM catalytic cycle of light and heavy paraffins is represented in Fig. 1 for a heavy alkane (ideally PE or PP) with a light alkane (such as *n*-octane). First, the dehydrogenation catalyst is responsible for the dehydrogenation of both the PE/heavy alkane and the light alkane added in excess to the system, resulting in the formation of unsaturated species. Afterwards, the olefin metathesis catalyst exchanges the saturated chains of these species, therefore shortening the initial PE/heavy alkane chain while increasing the chain of the lighter alkane. Posterior hydrogenation of the unsaturated species affords saturated alkanes,

* Corresponding author.
E-mail address: cmegias@us.es (C. Megías-Sayago).

https://doi.org/10.1016/j.apcatb.2023.123002
Received 24 February 2023; Received in revised form 28 May 2023; Accepted 14 June 2023
Available online 19 June 2023

closing the catalytic cycle. In order to successfully degrade the heavy alkane into short hydrocarbons, a large excess of light alkanes is necessary. Thus, initial CAM products react further with these light alkanes, being obtained shorter chain products that can be used as chemical feedstocks and/or synthetic fuels [10].

Several Ir pincer complexes have demonstrated to be active in alkane dehydrogenation reactions [9,12–15], being reported as highly regioselective for the terminal positions of *n*-alkanes [14,16]. However, for a more effective molecular weight reduction of the heavy alkane (PE) chain, olefin metathesis is required to occur at an internal C=C double bond [10]. The closer this double bond is to the middle of the polymer the more effective this CAM process will be. Fortunately, it has been reported that, under the reaction conditions, the terminal olefin is rapidly converted into internal olefins through isomerization [17,18], thus increasing the efficiency of the process.

In comparison to ($^{t\text{-Bu}}$PCP)Ir complexes, Brookhart's bis (phosphinite)-ligated ($^{t\text{-Bu}}$POCOP)Ir complex has demonstrated to be more efficient for PE degradation, fact that appears to be related with a higher tendency of ($^{t\text{-Bu}}$POCOP)Ir complexes to form internal alkenes during dehydrogenation [10]. In fact, the iridium complexes seem to play an important role in controlling the products distribution, being (POCOP)Ir based catalysts more effective to produce gaseous/oil range hydrocarbons (C_3-C_{42}) instead of waxes (C_{42+}) [10]. Within the possible (POCOP)Ir complexes, (p-^{t}-Bu_2PO-$^{t\text{-Bu}}$POCOP)Ir(C_2H_4) (see Fig. 1) had demonstrated a great activity towards alkane dehydrogenation [9,14] reason why it was chosen in this study.

The catalyst heterogenization through the complex immobilization on a support lead to a more robust catalyst, more stable thermally and easily recoverable, which enables its recyclability [19]. In this way, no ligand functionalization is needed to heterogenize the organometallic system which entails an important advantage [20]. The support can act not just as an inorganic carrier but also can participate in the catalytic reaction thus playing a pivotal role in the process, controlling the products distribution, potentiating preferential pathways and/or enhancing the rate-limiting step of a reaction [21,22], fact that will depend on the support nature. The complex' immobilization can be accomplished through the covalent attachment to an inorganic oxide surface, for instance. In this sense, many complexes have been grafted mostly in silica (or SBA-15) [15,20] and γ-Al_2O_3[10,14], finding application in different catalytic processes.

In the present study, Al_2O_3 and SiO_2 have been likewise used as supports (α-Al_2O_3 in this case) to immobilize the (p-^{t}-Bu_2PO-$^{t\text{-Bu}}$POCOP)Ir(C_2H_4) complex along with TiO_2 and three zeolites: mordenite and two ZSM-5 samples with different SiO_2/Al_2O_3 molar ratio, respectively. The complex grafting over the supports has been confirmed by FTIR spectroscopy and the support effect evaluated in the cross-alkane metathesis of *n*-dodecane and *n*-octane, molecules acting as models of heavy (polyethylene) and light alkanes, respectively. Additionally, the supports have been dehydroxylated at different conditions to evaluate its possible impact in the catalytic reaction. To the best of our knowledge, this is the first time that both support nature effect and support dehydroxylation effect are systematically evaluated in the degradation of heavy alkanes through CAM with light alkanes over supported pincer-ligated iridium complexes.

2. Experimental section

2.1. General considerations

All manipulations, synthesis and reactions were carried out under nitrogen using standard Schlenk-type techniques, Fisher-Porter bottle techniques and a Braun Labmaster 100 glovebox. All solvents were likewise distilled under nitrogen (diethyl ether, pentane, tetrahydrofuran and toluene) using appropriate desiccants: sodium benzophenone-ketyl for tetrahydrofuran (THF), and sodium for toluene and pentane. All other reagents were commercially available (Sigma Aldrich) and used as received.

2.2. Characterization techniques

NMR spectra were recorded on Bruker DPX-300, DRX-400, AVANCEIII/ASCEND 400 R or DRX-500 spectrometers, respectively. ^{1}H shifts were referenced to the residual signals of deuterated solvents while ^{31}P{^{1}H} NMR shifts were referred to external 85 % H_3PO_4. NMR measurements were performed at 25 ºC, being the data reported in ppm downfield from Me_4Si.

X-Ray diffractograms of the supports were recorded on a PANalytical X´Pert Pro diffractometer using Cu Kα radiation (40 mA, 45 kV, λ = 1.5406 Å) in a 2Θ range between 5 and 90º, using a step size of 0.05º and step time of 300 s

The iridium contents of all supported catalysts were measured by inductively coupled plasma atomic emission spectroscopy (ICP), being the complex wt% indirectly determined from this value. The measurements were carried out in a Horin Jobin Yvon ICP spectrometer, being the samples previously digested in HF.

The rhenium content of the metathesis catalyst, *i. e.* Re_2O_7/Al_2O_3,

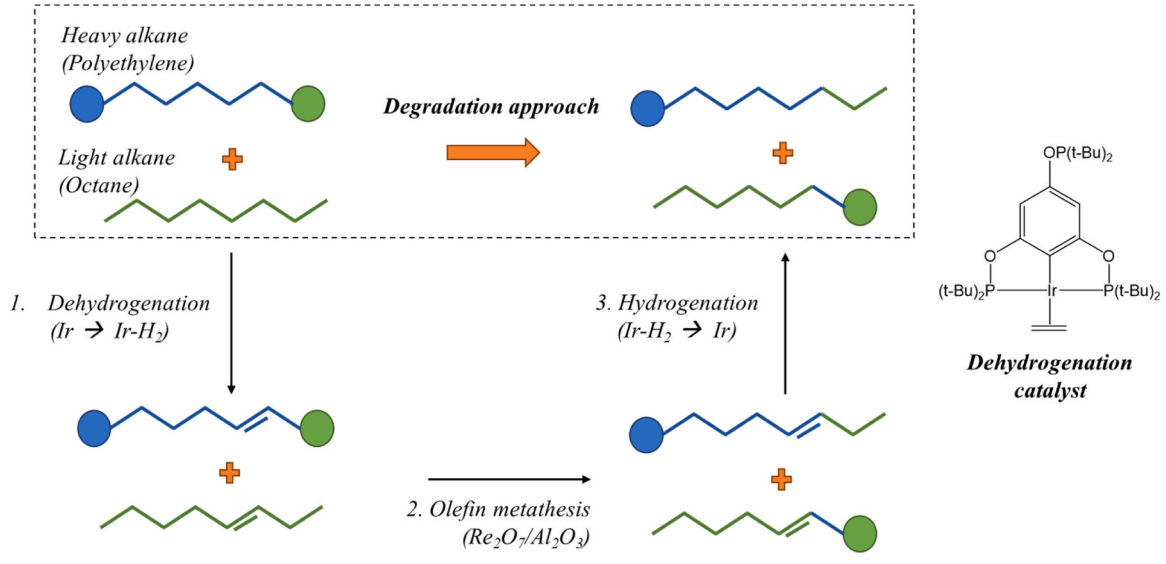

Fig. 1. Degradation of heavy alkanes through CAM with light alkanes: reported catalytic cycle and structure of the dehydrogenation catalyst used in this study.

was determined by X-ray fluorescence (XRF) using a Panalytical AXIOS spectrometer with Rh tube of radiation.

Nitrogen physisorption at 77 K was used to evaluate the textural properties of the supports which were degassed for 2 h at 250 ºC prior to the analysis. The measurements were carried out in a Micromeritics TRISTAR II equipment.

FTIR spectroscopic measurements were performed in diffuse reflectance mode using a high-temperature *in situ* DRIFT cell equipped with ZnSe windows and supported in a Praying Mantis optical system (Harrick). In order to ensure the required inert atmosphere, the DRIFT chamber was decoupled from the IR spectrometer and introduced inside the glovebox. The sample was then placed inside the chamber without packing or diluting, the chamber was perfectly closed and coupled again to the spectrometer. The samples were evaluated at room temperature after vacuum or by feeding a diluted CO stream (5 v/v % CO/He) through the cell during approximately 10 min and recording afterwards one spectrum. The IR spectra were recorded at 4 cm^{-1} of spectral resolution and an average of 64 scans per spectrum using a Thermo Nicolet iS50 FTIR spectrometer with KBr optics and MCT detector cooled at liquid N_2 temperature. All surface spectra were corrected with respect to a background spectrum previously collected with an aluminum mirror.

2.3. Synthesis of {p-OP(t-Bu)$_2$-C$_6$H$_2$-2,6-[OP(t-Bu)$_2$]$_2$}Ir(C$_2$H$_4$) complex and grafting in different supports

The {*p*-OP(t-Bu)$_2$-C$_6$H$_2$-2,6-[OP(t-Bu)$_2$]$_2$}Ir(C$_2$H$_4$) complex was synthetized as previously reported [14]. A scheme summarizing the synthesis steps has been included in the Supporting Information file (SI, Scheme S1).

^{1}H NMR (400 MHz, C_6D_6): δ 1.11 (d, $^3J_{PH} = 11.0$ Hz, 18 H, 2 x *t*-Bu), 1.23 (virtual triplet, apparent $J = 6.7$ Hz, 36 H, 4 x *t*-Bu), 3.11 (s, 4 H, C_2H_4), 7.04 (s, 2 H, 3- and 5-H). $^{31}P\{^1H\}$ NMR (400 MHz, C_6D_6): δ 150.6 (s, uncoordinated P(*t*-Bu)$_2$), 181.0 (s, coordinated 2 x P(*t*-Bu)$_2$).

The porous supports used in this study were α-Al_2O_3 (Sasol), TiO_2 (Alfa Aesar), SiO_2 (Evonik), Mordenite (with SiO_2/Al_2O_3 molar ratio equal to 20, from Zeolyst), ZSM-5_80 (with SiO_2/Al_2O_3 molar ratio equal to 80, original name CBV8014, from Zeolyst), ZSM-5_23 (with SiO_2/Al_2O_3 molar ratio equal to 23, original name CBV2314, from Zeolyst). Prior to the grafting, the supports were thermally treated at 500 ºC during 3 or 16 h (2 ºC/min) under vacuum in order to remove the physisorbed water and reduce the density of surface hydroxyls. The three zeolitic samples in their ammonium form were previously calcined in static air at 550 ºC during 15 h (10 ºC/min) to achieve their corresponding acidic structure.

The Ir complex was grafted on the different supports by using an adapted method from previous studies [14]. The Ir complex was first dissolved in 20 ml of pentane, this solution was then filtered and transferred to a Schlenk containing 1 g of the corresponding support (2 wt% nominal complex loading). The suspension was stirred at room temperature for 2 h. During this time, the red-colored solution lost its tonality in favor of the support. After that, the supported catalyst was washed with pentane repeatedly, dried under vacuum and finally stored. The supported samples were labelled as, for instance, Ir-C/ Al_2O_3_3 h where Ir-C, Al_2O_3 and 3 h indicate the presence of Ir complex, the type of support and the time used for dehydroxilation, respectively.

2.4. Synthesis of 5 % Re_2O_7/α-Al_2O_3

The metathesis catalyst was prepared adapting a previous reported synthesis [12]. NH_4ReO_4 (0.60 g, 2.24 mmol) was dissolved in 15 ml of distilled water, then 10 g of α-Al_2O_3 were added and the mixture stirred at room temperature for 15 min. The solvent was then eliminated in a rotary evaporator. The obtained solid was finally calcined at 550 ºC during 3 h (heating rate 10 ºC/min) under pure oxygen flow (30 ml/min).

2.5. Catalytic reactions

CAM reactions were carried out in Fisher–Porter vessels charged in a glovebox. In a typical reaction, the dehydrogenation catalyst (780 mg of supported complex), a mixture of alkanes (1.25 ml of *n*-octane and 1.25 ml *n*-dodecane, respectively), the metathesis catalyst (5 wt% Re_2O_7/Al_2O_3, 500 mg) and mesitylene (internal standard) were added to the Fisher–Porter reactor which was perfectly closed and heated at 175 ºC during 7 days, maintaining a stirring rate of 900 rpm. Once finished, a liquid aliquot was taken from the reaction mixture, microfiltered and analyzed. Products identification was carried out in a Shimadzu GC-2010 Chromatograph equipped with a Sh-rxi-5 ms column and coupled to a Shimadzu GCMS-TQ8040 mass spectrometer. Products quantification was performed in a Shimadzu GC-2010 Pro Chromatograph equipped with the same column. The concentration of each product was obtained directly from the peak areas, using the previously calibrated response factors.

3. Results and discussion

The X-ray diffractograms (XRD) of commercial supports are presented in Fig. 2a). Just briefly, SiO_2 shows a broad signal indicating low degree of crystallinity for this sample in contrast to the rest of supports. TiO_2 diffractogram corresponds to the anatase crystalline phase belonging to the tetragonal system (ICSD #01-071-1166). The alumina pattern can be attributed to α-Al_2O_3 (ICSD #01-071-1166, #00-047-1770 and #01-075-0921). Mordenite XRD matches to the pattern with empirical formula $Na_{0.3}(Al_{3.55}Si_{42.72}O_{96})\cdot(H_2O)_{2.76}$ (ICSD #01-080-0645) which corresponds to the orthorhombic crystal system. As for the two ZSM-5 zeolites both diffraction patterns are identical and confirm the sole presence of the MFI structure [23,24] along with high crystallinity degree in all cases.

Similarly, XRD patterns of metathesis catalyst, 5 %Re_2O_7/Al_2O_3 and its corresponding support (same α-Al_2O_3 described previously) are shown in Fig. 2b). The catalyst exhibits exactly the same diffractions than the support, none of the characteristic reflections of either Re_2O_7 and/or precursor (NH_4ReO_4) were observed in the XRD of the calcined sample which is in good agreement with previous reports [25–27]. Although some authors attributed this to the possible loss of rhenium oxide, which is volatile above 300 ºC, XRF results shown that real Re contents were really close to the nominal values [27] which is also our case (see Table 2). In this sense, Okal *et. al* [25] studied the behavior of Re_2O_7 and NH_4ReO_4 (supported in alumina) at different calcination temperatures and concluded that the precursor is oxidized to Re_2O_7 between 200 and 300 ºC with its instantaneous sublimation followed by adsorption and dissociation on the support as $(ReO_4)^-$ species. At 550 ºC (our calcination temperature), these $(ReO_4)^-$ species appears to form two different types of surface compounds, Al–O–ReO_3 and Al–(O–ReO_3)$_3$ structure, which are not visible by XRD, along with Re–O–Re bonds typical of Re_2O_7 [25]. In general, it has been accepted that less than 1 % of the rhenium ions form active species [28], that is, Re–O–Re surface species, being this the reason of the absence of diffractions.

The textural properties of all used supports and metathesis catalyst are summarized in Table 1 and the isotherms in Fig. S1 of the Supporting Information (SI) file. In general, supports can be divided in two groups, the mesoporous (Isotherm type IV) and the microporous ones (Isotherm type I), respectively. In the first group, SiO_2, TiO_2 and Al_2O_3 with BET surface areas of 213, 111 and 95 m^2/g, respectively. Within the samples, SiO_2 possesses the higher pore size and volume according also to its higher surface area, TiO_2 and Al_2O_3, for its part, have similar pore features. Compared to them, the used zeolites, Mordenite and both ZSM-5, have much higher surface areas (around 400 m^2/g of microporous surface) and lower pore sizes. As for 5 %Re_2O_7/Al_2O_3, the surface area is lower compared to the support along with the pore size and volume which indicates that rhenium oxide species are within the pores. The corresponding supported iridium complexes were not subjected to N_2

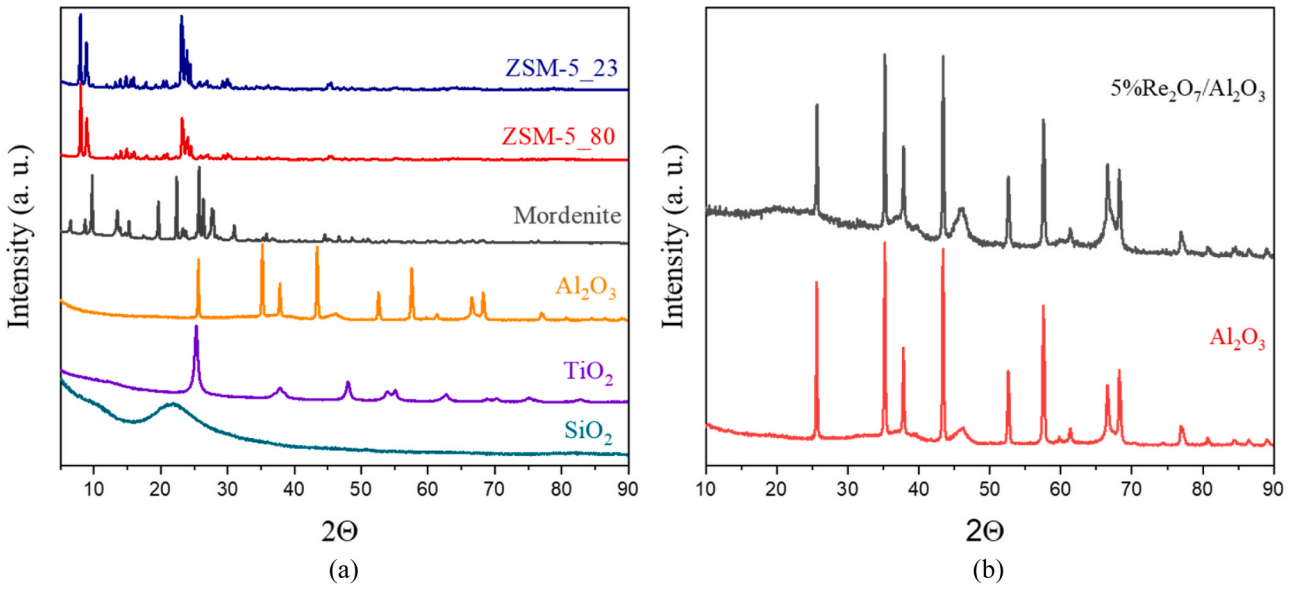

Fig. 2. a) XRD of used supports and b) XRD of the metathesis catalyst compared to its corresponding support.

Table 1
Textural properties of supports and metathesis catalyst, respectively.

Supports	S_{BET} (m^2/g)	Pore size (Å)	Pore volume (cm^3/g)	t-plot external surface area (m^2/g)	t-plot micropore area (m^2/g)
SiO_2_3h	213	138	0.77	205	9
TiO_2_3h	111	84.2	0.23	111	0
Mordenite_3h	452	77.9	0.24	55	397
Al_2O_3_3h	95	85	0.20	91	4
ZSM-5_23_3h	335	42	0.18	76	258
ZSM-5_80_3h	422	38	0.24	179	243
Re_2O_7/Al_2O_3	79	80	0.16	75	3

physisorption experiments due to the impossibility to carry out the measurements in total absence of air. As will be discussed below, the iridium complex considered in this study is unstable to air exposure.

The thermal treatments performed over the samples under vacuum aim to reduce the quantity of surface hydroxyls as a tool to attain a better complex dispersion over the support surface. This hydroxyls density decrease was evaluated by DRIFT, decoupling the chamber from the IR spectrometer, and introducing it inside the glovebox to deposit the sample. The difference FTIR spectra obtained after Al_2O_3 dehydroxylation during 3 or 16 h at 500 ºC are presented in Fig. 3a, showing the 3400 – 3900 cm^{-1} region. Similar to that reported in the literature [29,30], the samples treatment not only dehydroxylates the surface but also removes first adsorbed water. During the dehydroxylation process, proton acceptor OH groups (Brönsted base) are combined with proton donor OH groups (Brønsted acid) leading to the formation of a water molecule that desorbs from the support's surface. The disappearance of bands at 3791, 3773, 3737, 3723, and 3692 cm^{-1} which have been assigned to $(Al_{VI})OH$, $(Al_{IV})OH$, $(Al_{VI})_2OH$, $(Al_{IV}Al_{VI})OH$ and $(Al_{VI})_3OH$ [31], respectively, is evidenced for both samples Therefore, five types of OH species are differentiated on the alumina surface which depends on both the number of Al^{3+} bonded to the OH group (one, two or three) and the coordination number of the Al^{3+} ion (IV or VI) [31–33]. The bands disappearing after 16 h of treatment are exactly the same described above for 3 h. Although the hydroxyls density does not apparently vary, the difference spectra of both samples (Fig. 3b) shows that increasing the time from 3 to 16 h reduces even more the hydroxyls. Nevertheless, the support dehydroxylation mostly occurs at the beginning of the thermal treatment.

As the surface hydroxyls density will be different for each support, the behavior as function of time may change for each particular case. Nevertheless, for easy of comparison, the same treatment was applied to all the used supports.

The complex was then grafted on the supports through wet impregnation with pentane as solvent. As reported previously [15,20], the complex-support interaction is usually established through a covalent bond and the surface hydroxyl groups of the supports have been demonstrated to play a key role in its formation [34]. The difference spectra (dehydroxylated support/grafted complex) of all samples are presented in Fig. 4. The 2800–4000 cm^{-1} region comprises the O-H and C–H stretching regions which gives us information about the hydroxyls involved in the grafting process along with the presence of complex in the samples. The latter is evidenced by the bands situated between 2800 and 3000 cm^{-1} in all samples which corresponds to the C-H stretching vibrational modes of the complex. The bands disappearing in the hydroxyls' region, concretely between 3600 and 3800 cm^{-1}, can be attributed to the hydroxyls that disappear as consequence of the oxygen interaction with the complex during the grafting.

The bands decreasing after the grafting on alumina are the same identified above, 3791, 3773, 3737, 3723, and 3692 cm^{-1} previously assigned to $(Al_{VI})OH$, $(Al_{IV})OH$, $(Al_{VI})_2OH$, $(Al_{IV}Al_{VI})OH$ and $(Al_{VI})_3OH$ [31]. It can be deduced that grafting takes places in all the hydroxyl species differentiated for the support. The hydroxyl bands are not that clear for Ir-C/SiO_2_3h sample, just a slight decrease in a band situated at 3747 cm^{-1}, assigned to isolated silanols vibration [35], is poorly noted. Nevertheless, the bands attributed to C–H vibrations are clearly observed which suggest that the complex is present thus interacting somehow with the support, most probably through electrostatic forces (physisorption). Analyzing separately the support and supported complex spectra (Fig. S2) it is clear that the band corresponding to isolated silanols vibration (situated at 3747 cm^{-1}) remains unaltered. Differently, Ir-C/TiO_2_3h sample exhibits clear negative bands in the hydroxyl region, concretely 3710, 3693, 3670 and 3648 cm^{-1}, which have been previously attributed to four types of hydroxyl species of anatase, *i. e.* bridging OH (3710 cm^{-1}), H-bonded terminal OH (3693 and 3648 cm^{-1}) and isolated terminal OH (3670 cm^{-1}) [36]. The negative bands observed for Ir-C/ZSM-5_23_3h sample are situated at 3747, 3670, 3650 and 3620 cm^{-1} which have been ascribed to isolated silanol (Si–OH) groups, extra-framework aluminum OH-μ_2-Al species and Si–O(H)–Al Brønsted acid sites, respectively [37]. The latter demonstrated that the complex is also interacting with the acid sites in the zeolite thus

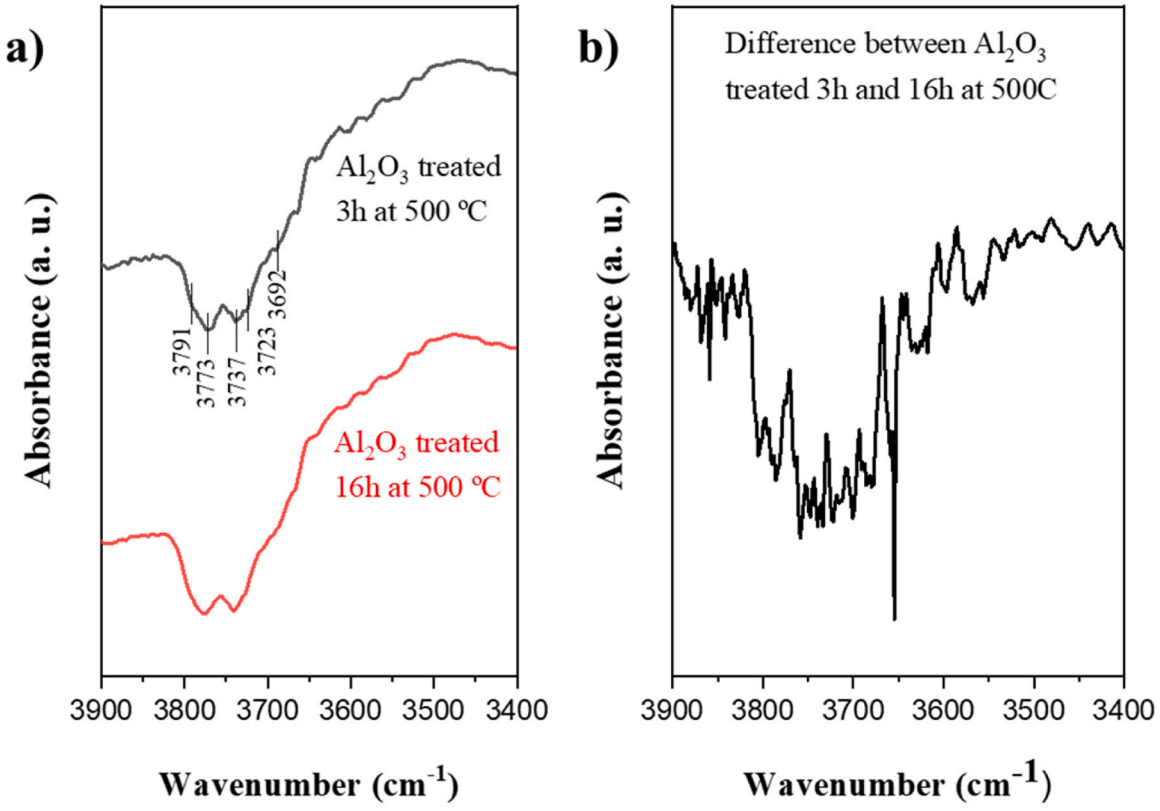

Fig. 3. a) Difference FTIR spectra recorded after Al_2O_3 dehydroxylation during 3 or 16 h at 500 ºC b) Difference FTIR spectra between both samples treated at 500 ºC during 3 or 16 h, respectively.

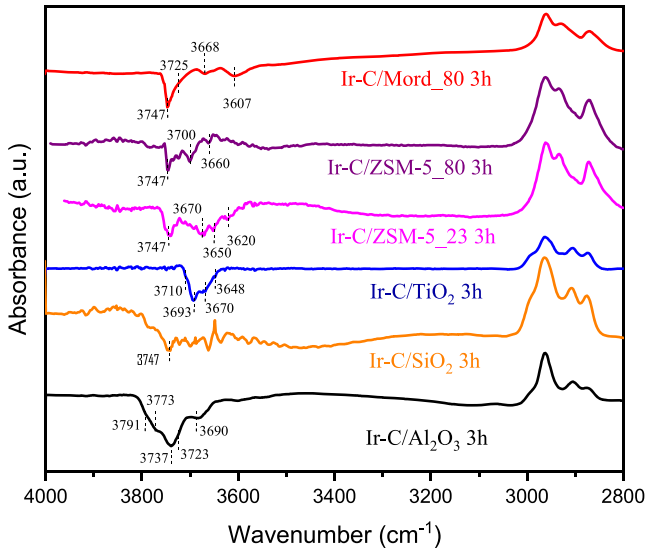

Fig. 4. Difference FTIR spectra recorded after the complex grafting over each support (previously dehydroxylated during 3 h at 500 ºC).

diminishing its Brønsted acidity once grafted. The hydroxyl bands associated to Ir-C/ZSM-5_80_3h sample are slightly different that its analogous MFI zeolite, the band at 3620 cm^{-1} ascribed to one type of Si–O(H)–Al Brønsted acid sites does not appear which seems logical considering that this zeolite is less acid. In its place, a new band situated at 3700 cm^{-1} is observed for this sample which has been also attributed to extra framework aluminium species [38]. Finally, for the Ir-complex supported on mordenite, four bands are clearly detected at 3747, 3725, 3668 and 3607 cm^{-1} which have been assigned to isolated and internal (Si–OH) groups (3747, 3725 cm^{-1}), extra-framework aluminium species (3668 cm^{-1}) and Si–O(H)–Al Brønsted acid sites (3607 cm^{-1}) [39].

In summary, the presence of different negative bands in the O–H region after the grafting inform about the interaction of specific surface hydroxyl groups of supports with the complex. The presence of the latter in all samples have been revealed by the positive bands in the C–H region. The complex has shown to interact with different hydroxyl groups in the samples, that is, the interaction does not appear to be selective which in principle should lead to a good dispersion over the support.

The possible structures for the covalently anchored supported complex are presented in Scheme 1, including not only the complex considered in this study (route B) but also the one without *para*-substituent (route A) and the precursor of our final complex, *i.e.* the chlorohydride Ir complex that is obtained before introducing ethylene (route C, see Scheme S1 compound 3).

The interaction of the complex with the support depends either on the presence of a basic functional group in the *para*-position (like a phosphinite group) of the pincer and on the Ir co-ligands [9,15,40]. As demonstrated by solid-state ^{31}P MAS NMR [15,20], in absence of a basic *para*-substituent the interaction occurs through the iridium center which becomes Ir(III) as schematized in Scheme 1A. This kind of interaction also depends on the Ir co-ligands even when the complex has a basic *para*-substituent on the pincer (Scheme 1C), being the complex also bonded to the support through the iridium center. In both cases, the support is treated as a ligand, approach known as surface organometallic chemistry (SOMC) [34], the iridium oxidation state changing from Ir(I) to Ir(III) after grafting. Contrary, the ethylene complex has demonstrated to be anchored through the *para*-position, losing a phosphinous acid group [15,40]. The Ir remains as Ir(I) thus its reactivity is not affected in principle by the support presence. All supported species evolve to carbonyl Ir complexes in the presence of CO as schematized above.

In this regard, the CO vibrational bands can serve us to elucidate

Scheme 1. Proposed grafting of A){C_6H_2-2,6-[OP(t-Bu)$_2$]$_2$}Ir(C_2H_4), B) {*p*-OP(t-Bu)$_2$-C_6H_2-2,6-[OP(t-Bu)$_2$]$_2$}Ir(C_2H_4) and C) {*p*-OP(t-Bu)$_2$-C_6H_2-2,6-[OP(t-Bu)$_2$]$_2$} IrH(Cl) on alumina and species evolution in presence of CO.

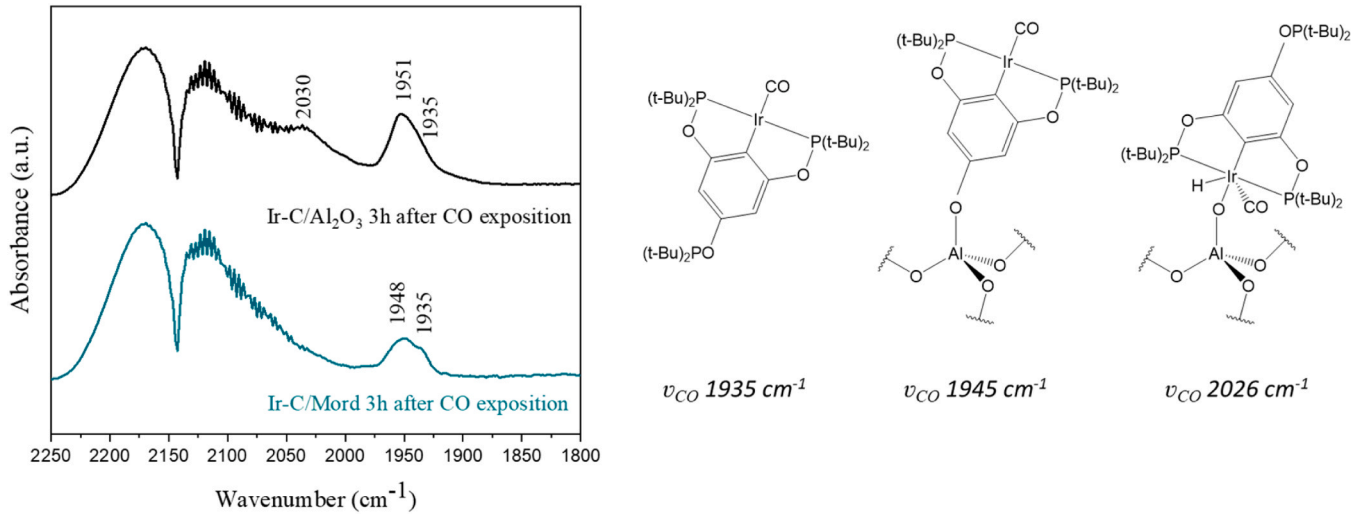

Fig. 5. Representative FTIR spectra recorded after exposure of supported complexes to CO. Possible CO-containing species depending on the anchoring.

which kind of CO-containing complexes are present in the supported samples since vibrational frequency changes [15,40,41]. Fig. 5 displays the spectra recorded after passing diluted CO (5 v/v % CO/He) through two representative samples along with the possible CO-containing species depending on the anchoring. The IR spectra show that the reaction between Ir centers and CO is instantaneous, forming several iridium carbonyl complexes (positive bands situated at 1935, 1948–1951 and 2030 cm^{-1}, respectively). Gaseous CO is also rapidly observed (negative band centered at 2143 cm^{-1}). The band around 1948–1951 cm^{-1} is the most intense in all samples which is ascribed to the supported iridium(I) carbonyl complex represented in Scheme 1 Route B [15,20,40]. Furthermore, a smaller band at 1935 cm^{-1} is observed in all cases, attributed to non-supported iridium(I) carbonyl complex [15,20,40] which remains most probably physisorbed. Finally, a weak band is detected at 2030 cm^{-1} in some cases which accounts for supported iridium(III) carbonyl complex formation. The latter may be expected considering that the conversion of complex 3 in complex 4 (Scheme S1) was not complete (residual signals of the iridium hydride were detected in ^1H NMR). Nevertheless, the grafted iridium(III) carbonyl complex has been reported to undergo reductive elimination to unsupported Ir(I) complex [15,20,40]. Therefore, the ethylene complex with *para*-substituent binding appears to inhibit a decomposition reaction of the iridium center with the support.

Table 2 arranges all ICP and XRF values obtained for the samples, including both the supported iridium complexes and the metathesis catalyst. In addition to the supports thermally treated during 3 h at 500 ºC under vacuum, the iridium complex was likewise supported over non previously treated α-Al_2O_3 (labelled as Al_2O_3_NT) and alumina dehydroxylated at the same temperature but during 16 h (Al_2O_3_16h). Regarding the iridium complex loading, it was indirectly calculated from the Ir percentage obtained by ICP. In general, the real complex loading was lower than the targeted 2 wt% in all samples, being the loading of Ir-C/TiO_2_3h (1.91 wt%) the closest to the nominal, followed by Ir-C/Al_2O_3_3 h, Ir-C/Mord_3h and Ir-C/ SiO_2_3h, respectively. This trend could be explained attending to the hydroxyls population after the thermal treatment which will be logically different depending on the support. The lowest value registered for Ir-C/ SiO_2_3h is not surprising since all the complex appears physisorbed or at least not interacting *via* hydroxyls. Comparing the alumina supported samples, one may expect that the hydroxyls density decreases with the thermal treatment, that is, in the following order: Al_2O_3_NT > Al_2O_3_3h > Al_2O_3_16h, this trend being indirectly proportional to the iridium complex loading. However, experimentally it is observed that the highest loading is achieved over the sample dehydroxylated during 3 h, the other two values being lower and similar. The complete dehydroxylation (Al_2O_3_16h) and the water-hydroxyls interaction for the NT sample decrease the number of anchoring centers resulting in less Ir complex attachment and, as consequence, in low metal loadings. As for ZSM-5 samples, the grafted amount is lower in comparison with the rest of supports, except for SiO_2, the Ir loading being higher in the less acidic zeolite. Although the complex is interacting with Brönsted acid sites (Si–O(H)–Al), those sites might be sterically less accessible than silanols and extra-framework aluminum thus diminishing the amount of grafted complex.

Finally, Re loading was measured by XRF and considered 100 % Re_2O_7 to calculate the weight percentage. As tabulated, rhenium oxide amount is higher than the target (5 wt%). The latter could be related with some support lost during the dissolution and/or the calcination treatment in pure oxygen at 550 ºC.

The catalytic activity of all samples was evaluated in the cross-alkane metathesis of *n*-dodecane (heavy alkane model molecule) with *n*-octane (light alkane). In this reaction, the Ir supported samples are expected to dehydrogenate both the heavy alkane (which would be ideally polyethylene) and the light alkane (that would be solvent and reagent), resulting in the formation of unsaturated species. Subsequently, the olefin metathesis catalyst is responsible for the exchange of the saturated chains thus reducing/increasing the heavy/light alkane chain, respectively. The expected products are alkanes of different carbon numbers, obtained after hydrogenation mediated by the iridium hydride species. In this context, evaluating the possible influence of support nature and support treatment can be crucial to properly design active catalysts. The support may not only act as inorganic carrier but also may have a pivotal role in controlling the products distribution since it can participate in the catalytic reaction. Indeed, both the anchored complex and the support could work cooperatively to yield synergetic results, which can be highly desirable depending on the target. Therefore, the complex immobilization on a support is not only interesting due to its heterogenization (with all the advantages that entails) but also to the possible modulation of the complex's catalytic activity which will depend on the support nature. Support dehydroxylation, on the other hand, intents to improve the complex dispersion on the support surface by reducing the hydroxyls density. The immobilization of 'more isolated' species aims to enhance the catalyst activity.

The possible effect of thermal treatment on the catalytic activity of Ir-C/Al_2O_3 catalysts was evaluated, and the results presented in Fig. 6 (see Fig. S3 for GC trace analysis of a post reaction mixture). The treatment during 3 h under vacuum conduces to the best results being the CAM process clearly evidenced by the wide distribution of lineal alkanes produced, higher and lower in C number from the initial ones which implies successive alkane dehydrogenation, metathesis and hydrogenation, respectively. Reactions were performed without any hydrogen acceptor and control experiments were carried out to validate that any product is found without the Ir supported catalysts and just the corresponding alkenes were visible in absence of metathesis catalyst. No branched or cyclic alkanes were detected except for C4 where alkane isomers and even alkenes were observed. In general, a Gauss-type distribution (C4 to C30 for the best sample) is obtained with higher concentration of C9 to C11 which agrees with the reported mechanism for this reaction [9,10,12]. Nevertheless, the exact mechanism appears controversial regarding the selective (or not) dehydrogenation of the used Ir complex to terminal alkane positions. Goldman *et. al* [12] stated that CAM process undergoes through terminal alkane dehydrogenation followed by alkene isomerization and metathesis which would explain the observed products range. Jia *et. al* [10] hypothesized that the dehydrogenation catalyst should favor the formation of internal olefins, being more efficient for PE degradation, since they observed high degradation degree of even commercial PE. In any case, to the aim of this study, the positive effect induced by the support treatment is clear. Even considering the complex loading, which is higher for Ir-C/Al_2O_3_3h but lower and equal for Ir-C/Al_2O_3_NT and Ir-C/Al_2O_3_16h, the catalytic activity of the last one is higher compared to the non-treated sample accounting most probably for a better dispersion of the complex on the support's surface.

The effect of the support on the catalytic activity of prepared catalysts was also studied and the screening results outlined in Fig. 7. Detected products concentrations strongly depend on the type of support and concretely on the support zeolitic character. While over α-Al_2O_3, TiO_2 and SiO_2 based catalysts (Fig. 7a) the products distribution follows

Table 2
ICP and XRF values obtained for all supported samples.

Catalyst	Ir (complex) loading (ICP, % wt.)		Re_2O_7 loading (XRF,% wt.)
	Ir	Ir-complex	
Ir-C/ SiO_2_3h	0.19	0.78	-
Ir-C/TiO_2_3h	0.48	1.91	-
Ir-C/Mord_3h	0.31	1.24	-
Ir-C/Al_2O_3_3h	0.33	1.32	-
Ir-C/Al_2O_3_16h	0.29	1.17	-
Ir-C/Al_2O_3_NT	0.28	1.12	-
Ir-C/ZSM-5_23_3h	0.15	0.62	-
Ir-C/ZSM-5_80_3h	0.24	0.96	-
Re_2O_7/Al_2O_3	-	-	10.9

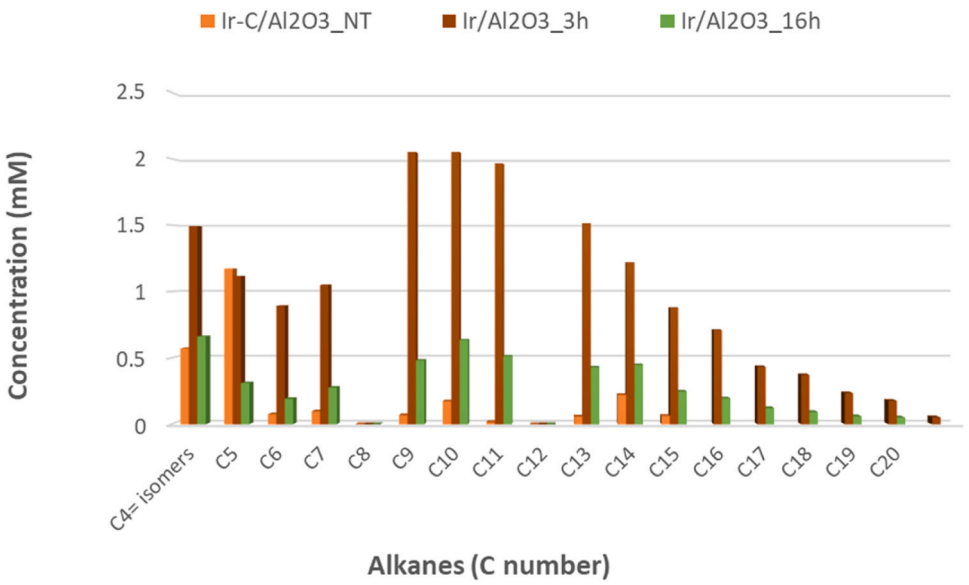

Fig. 6. Cross metathesis of *n*-dodecane (4.36 M, 1.25 ml) with *n*-octane (6.03 M, 1.25 ml) using the Ir complex (20 μmol) grafted on differently treated α-Al_2O_3 and Re_2O_7/α-Al_2O_3 (500 mg) after 7 days at 175 °C. Note: the concentration of the initial alkanes (C8 and C12) is not included.

practically the trend described above, the zeolitic based catalysts (Fig. 7b) behave different. The first aspect standing out is the concentration of obtained products, more than 50 times higher, which might be a signal of support participation in the reaction. In addition to this, C13 is the heaviest alkane observed which suggests that cross-alkane metathesis is not the only process undergoing during the experiments. In this sense, bare zeolites have demonstrated to degrade polyolefins through catalytic cracking [42,43], in absence of additional functionalities. This explains the much higher activity observed over the zeolite supports compared to α-Al_2O_3, TiO_2 and SiO_2. The immobilization of the Ir catalyst appears to have a modest impact on the reaction conversion, which would suggest that polymers upcycling by cracking over zeolites could be much more effective than alkane cross metathesis using Ir and Re based catalysts. Nevertheless, the presence of metathesis catalyst could enhance the zeolite intrinsic activity, a factor that need to be evaluated in detail. On the other hand, confinement effects are the most important features of zeolites and have been demonstrated to play a key role in confined noble-metal catalysts [44], therefore, its possible impact in the CAM process must be also considered.

As for the mesoporous supported systems, Ir-C/α-Al_2O_3_3h emerges as the best catalyst followed by Ir-C/TiO_2_3h and Ir-C/SiO_2_3h. The last two samples exhibit different products ratios, being the heavy fraction concentration higher over Ir-C/SiO_2_3h and the lighter over Ir-C/TiO_2_3h. The differences between supports could be related to different factors and, most probably, to a combination of them. Marczewski et al. [45] studied the alkane/alkene isomerization over modified Al_2O_3, TiO_2 and SiO_2 and demonstrated that the isomerization occurs over strong Lewis acid sites combined with close Brønsted acid sites and/or over strong Brønsted acid sites. Therefore, the acidic properties of supports must have a pivotal role in the CAM reaction, being the acid strength and the Lewis/ Brønsted ratio in the catalysts determinant to properly explain the obtained results. The availability and strength of those sites would depend not only on the support but also on support thermal treatment and on the immobilized complex. In addition, the complex dispersion over the supports might be another factor to consider.

In order to evaluate the possible participation of bare supports in the process, reactions were repeated in absence of grafted complex and the results are showed in Fig. 8. It should be noted that only alumina has been presented as representative sample of mesoporous supports since, as in the case of alumina, SiO_2 and TiO_2 supports do not lead to any product formation. This underlines that the iridium complex, in combination with the metathesis catalyst, are totally responsible for the cross metathesis of *n*-dodecane with *n*-octane although it does not rule out that the support can be participating in the process, for example, promoting the isomerization of terminal alkenes which would potentiate the alkane degradation [12]. In fact, the differences observed over the mesoporous samples might be tentatively ascribed to the acidic properties of catalysts as exposed above. Regarding the zeolite-based catalysts, the support is clearly active itself through catalytic cracking as reported for MFI type zeolites as well as for mordenite [46]. Nonetheless, the one having SiO_2/Al_2O_3 molar ratio of 23 appear to behave differently, the complex presence enhancing its catalytic performance. Although catalytic cracking is surely occurring, alkanes from C13 to C16 are observed which suggests that CAM process is undergoing in a higher extent when compared to its homologous aluminosilicates. The latter might be explained considering the acidic properties of both zeolites along with the grafted complex, which was covalently anchored on Brønsted sites (among other sites) thus diminishing the catalyst's acidity, as demonstrated by FTIR spectroscopy. In this sense, ZSM-5_23 is a more acidic zeolite than ZSM-5_80 thus, presumably, the amount of Brønsted sites after the complex grafting would be higher in this sample, potentiating the CAM process *via* isomerization of terminal alkenes. On the other hand, since ZSM-5_23 and Mordenite have almost the same SiO_2/Al_2O_3 ratio (23 and 20 for ZSM-5_23 and mordenite, respectively) the possible effect of different pore sizes might be tentatively considered and discussed. The pore system of mordenite involves channels of 6.5 × 7.0 Å, connected by pores of 2.6 × 5.7 Å while the MFI has two types of interconnected channels, with a diameter of 5.6 Å and 5.3 Å, respectively. In general terms, mordenite has larger channels than MFI but lower size of the pores connecting the channels, which presumably might be the explanation of the observed results. Mordenite led mostly to lighter alkanes whereas over ZSM-5_23 sample heavier hydrocarbons are detected in addition to a light alkanes fraction. The latter could be ascribed to the porous structure of both samples, mordenite has big enough channels to host heavy lineal alkanes but smaller pores connecting the channels, compared to ZSM-5, which might cause more cracking/CAM reactions thus diminishing the alkanes chain.

Although support participation relies on its nature, the effect of immobilizing the complex in different supports has been clearly underlined. Investigating the exact role of each support and how to enhance and/or modulate its participation in the catalytic reaction will definitively pave the way to the design of efficient heterogeneous

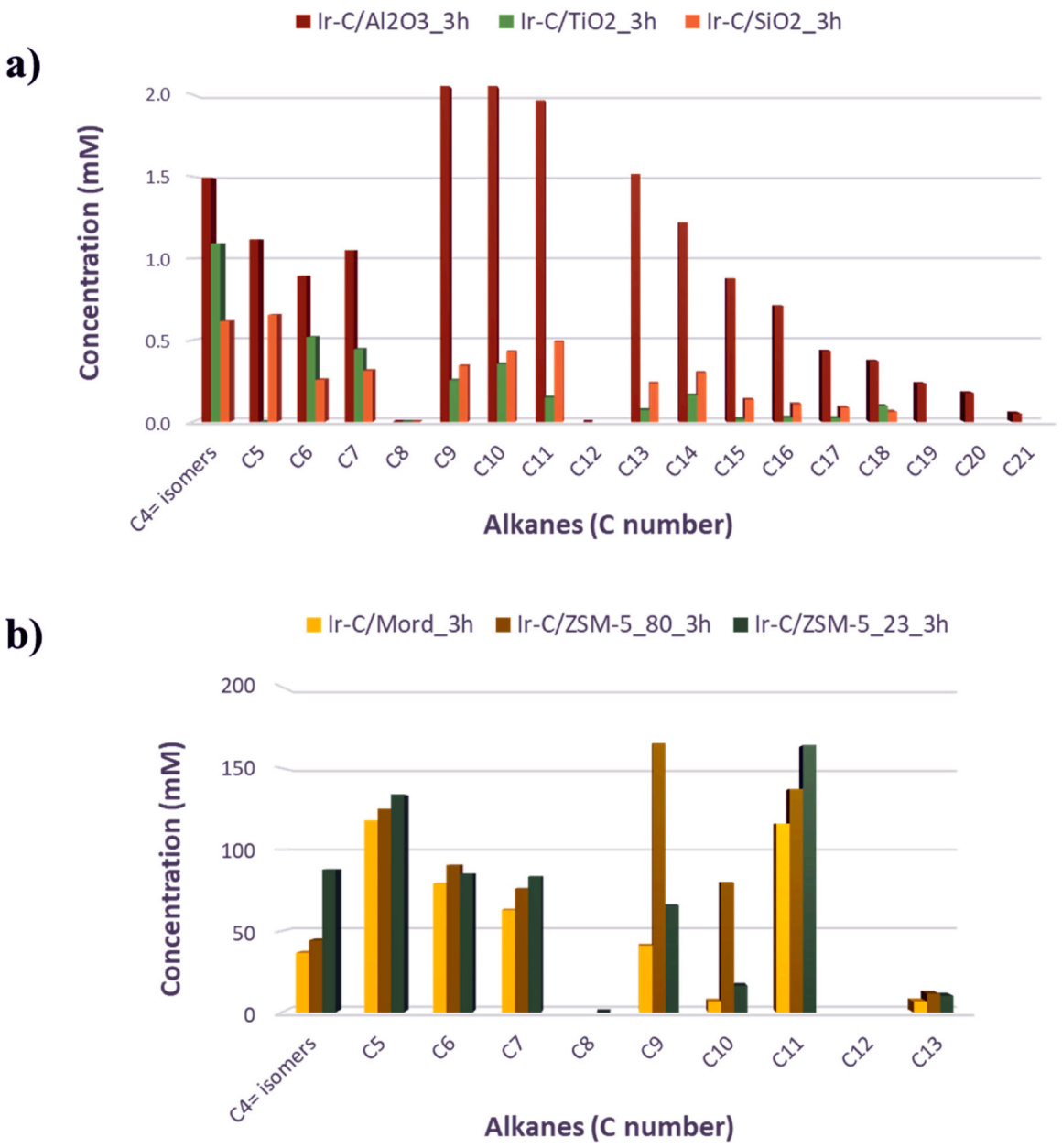

Fig. 7. Cross metathesis of *n*-dodecane (4.36 M, 1.25 ml) with *n*-octane (6.03 M, 1.25 ml) using the Ir complex (20 μmol) grafted on a) mesoporous supports and b) microporous supports and $Re_2O_7/\alpha\text{-}Al_2O_3$ (500 mg) after 7 days at 175 °C. Note: the concentration of the initial alkanes (C8 and C12) is not included.

catalysts for plastic upcycling.

4. Conclusions

The grafting of pincer-ligated iridium complexes over different inorganic supports has been successfully achieved as confirmed by FTIR spectroscopy. Several structures for the covalently anchored complex were considered, being the anchoring site elucidated thanks to the analysis of the corresponding carbonyl Ir complexes by FTIR (all the immobilized complexes evolved to carbonyl species in the presence of CO). Prior to the grafting, the used supports, meso and microporous (zeolitic) ones, were treated during different times at 500ºC under vacuum in order to reduce the density of surface hydroxyls, treatments that have been demonstrated to affect the catalytic performance in the alkane metathesis reaction. In fact, treating the support during 3 h led to the best supported system in terms of catalytic performance compared to the non-treated sample and the one thermally treated during 16 h. The influence of the support nature and its participation in the catalytic reaction have been clearly evidenced. Within the mesoporous supports ($\alpha\text{-}Al_2O_3$, SiO_2 and TiO_2), $\alpha\text{-}Al_2O_3$ stood up as the best, being the differences between the samples related most probably to the differences in support acidity (acid strength and Lewis/ Brønsted acid ratio). The zeolitic supports clearly contributed to the process, cracking the alkanes, thus being alkane cracking and metathesis undergoing for this samples. The results were dependent on the zeolite acidity and type, being the product distribution also connected to the zeolitic pore structure.

CRediT authorship contribution statement

Cristina Megías-Sayago: Conceptualization, Methodology, Data curation, Investigation, Writing – original draft, Writing – review & editing, Funding acquisition. **Ignacio Centeno-Vega:** Investigation, Data curation, Writing – original draft. **Luis F. Bobadilla:** Conceptualization, Methodology. **Svetlana Ivanova:** Conceptualization,

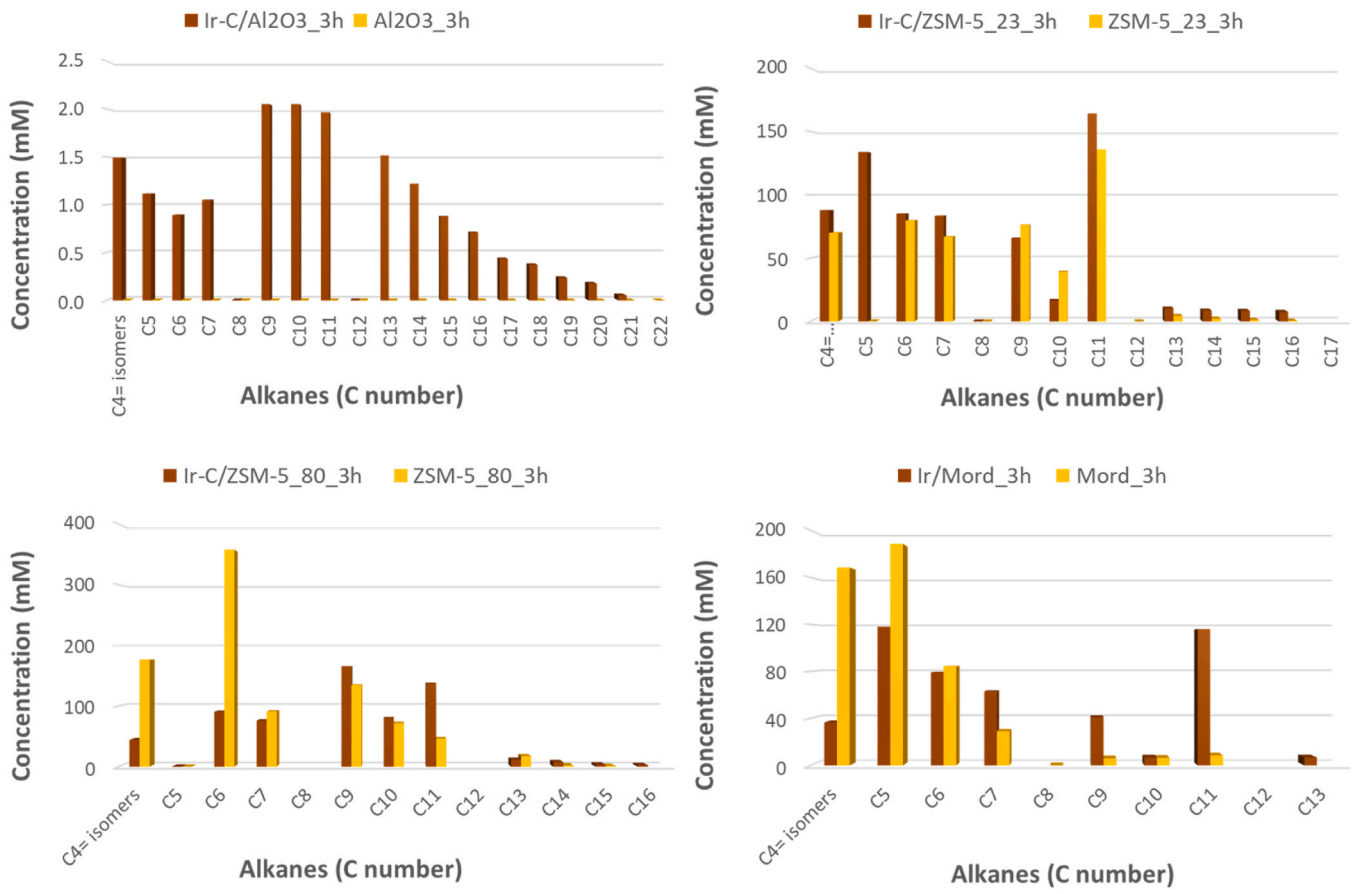

Fig. 8. Cross metathesis of *n*-dodecane (4.36 M, 1.25 ml) with *n*-octane (6.03 M, 1.25 ml) using the Ir complex (20 μmol) grafted on different supports and Re_2O_7/α-Al_2O_3 (500 mg) after 7 days at 175 °C: catalysts *vs.* supports. Note: the concentration of the initial alkanes (C8 and C12) is not included.

Methodology, Supervision. **Nuria Rendón:** Supervision, Funding acquisition. **Andrés Suarez:** Supervision, Funding acquisition.

Declaration of Competing Interest

The authors declare that they have no known competing financial interests or personal relationships that could have appeared to influence the work reported in this paper.

Data availability

Data will be made available on request.

Acknowledgements

C. Megías-Sayago acknowledges the European Union's Horizon 2020 Research and Innovation Programme for the funding received for this work under the Marie Skłodowska-Curie grant agreement No 101022598. N. Rendón and A. Suarez thank the financial support (FEDER contribution) from the Spanish Agencia Estatal de Investigación (PID2019–104159GB-I00/TED2021-129181B-I00), Junta de Andalucía (US-1380604) and CSIC (COOPB20604).

Appendix A. Supporting information

Supplementary data associated with this article can be found in the online version at doi:10.1016/j.apcatb.2023.123002.

References

[1] A.H. Westlie, E.Y.X. Chen, C.M. Holland, S.S. Stahl, M. Doyle, S.R. Trenor, K. M. Knauer, Polyolefin Innovations toward circularity and sustainable alternatives, Macromol. Rapid Commun. (2022), https://doi.org/10.1002/marc.202200492.
[2] G. Lopez, M. Artetxe, M. Amutio, J. Bilbao, M. Olazar, Thermochemical routes for the valorization of waste polyolefinic plastics to produce fuels and chemicals. A review, Renew. Sustain. Energy Rev. 73 (2017) 346–368, https://doi.org/10.1016/j.rser.2017.01.142.
[3] R. Geyer, J.R. Jambeck, K.L. Law, Production, use, and fate of all plastics ever made, Sci. Adv. 3 (2017), https://doi.org/10.1126/sciadv.1700782.
[4] J.C. Worch, A.P. Dove, 100th Anniversary of macromolecular science viewpoint: toward catalytic chemical recycling of waste (and future) plastics, ACS Macro Lett. 9 (2020) 1494–1506, https://doi.org/10.1021/acsmacrolett.0c00582.
[5] A. Rahimi, J.M. García, Chemical recycling of waste plastics for new materials production, Nat. Rev. Chem. 1 (2017) 0046, https://doi.org/10.1038/s41570-017-0046.
[6] G. Celik, R.M. Kennedy, R.A. Hackler, M. Ferrandon, A. Tennakoon, S. Patnaik, A. M. LaPointe, S.C. Ammal, A. Heyden, F.A. Perras, M. Pruski, S.L. Scott, K. R. Poeppelmeier, A.D. Sadow, M. Delferro, Upcycling single-use polyethylene into high-quality liquid products, ACS Cent. Sci. 5 (2019) 1795–1803, https://doi.org/10.1021/acscentsci.9b00722.
[7] A. Tennakoon, X. Wu, A.L. Paterson, S. Patnaik, Y. Pei, A.M. LaPointe, S.C. Ammal, R.A. Hackler, A. Heyden, I.I. Slowing, G.W. Coates, M. Delferro, B. Peters, W. Huang, A.D. Sadow, F.A. Perras, Catalytic upcycling of high-density polyethylene via a processive mechanism, Nat. Catal. 3 (2020) 893–901, https://doi.org/10.1038/s41929-020-00519-4.
[8] F. Zhang, M. Zeng, R.D. Yappert, J. Sun, Y.-H. Lee, A.M. LaPointe, B. Peters, M. M. Abu-Omar, S.L. Scott, Polyethylene upcycling to long-chain alkylaromatics by tandem hydrogenolysis/aromatization, Science 370 (2020) (1979) 437–441, https://doi.org/10.1126/science.abc5441.
[9] Z. Huang, E. Rolfe, E.C. Carson, M. Brookhart, A.S. Goldman, S.H. El-Khalafy, A.H. R. MacArthur, Efficient heterogeneous dual catalyst systems for alkane metathesis, Adv. Synth. Catal. 352 (2010) 125–135, https://doi.org/10.1002/adsc.200900539.
[10] X. Jia, C. Qin, T. Friedberger, Z. Guan, Z. Huang, Efficient and selective degradation of polyethylenes into liquid fuels and waxes under mild conditions, Sci. Adv. 2 (2016), https://doi.org/10.1126/sciadv.1501591.

[11] A.H. Westlie, E.Y.X. Chen, C.M. Holland, S.S. Stahl, M. Doyle, S.R. Trenor, K. M. Knauer, Polyolefin innovations toward circularity and sustainable alternatives, Macromol. Rapid Commun. 43 (2022), https://doi.org/10.1002/marc.202200492.
[12] A.S. Goldman, A.H. Roy, Z. Huang, R. Ahuja, W. Schinski, M. Brookhart, Catalytic alkane metathesis by tandem alkane dehydrogenation-olefin metathesis, Science 312 (2006) (1979) 257–261, https://doi.org/10.1126/science.1123787.
[13] K. Zhu, P.D. Achord, X. Zhang, K. Krogh-Jespersen, A.S. Goldman, Highly effective pincer-ligated iridium catalysts for alkane dehydrogenation. DFT calculations of relevant thermodynamic, kinetic, and spectroscopic properties, J. Am. Chem. Soc. 126 (2004) 13044–13053, https://doi.org/10.1021/ja047356l.
[14] Z. Huang, M. Brookhart, A.S. Goldman, S. Kundu, A. Ray, S.L. Scott, B.C. Vicente, Highly active and recyclable heterogeneous iridium pincer catalysts for transfer dehydrogenation of alkanes, Adv. Synth. Catal. 351 (2009) 188–206, https://doi.org/10.1002/adsc.200800615.
[15] B. Sheludko, M.T. Cunningham, A.S. Goldman, F.E. Celik, Continuous-flow alkane dehydrogenation by supported pincer-ligated iridium catalysts at elevated temperatures, ACS Catal. 8 (2018) 7828–7841, https://doi.org/10.1021/acscatal.8b01497.
[16] M.C. Haibach, S. Kundu, M. Brookhart, A.S. Goldman, Alkane metathesis by tandem alkane-dehydrogenation–olefin-metathesis catalysis and related chemistry, Acc. Chem. Res. 45 (2012) 947–958, https://doi.org/10.1021/ar3000713.
[17] W. Yao, Y. Zhang, X. Jia, Z. Huang, Selective catalytic transfer dehydrogenation of alkanes and heterocycles by an iridium pincer complex, Angew. Chem. 126 (2014) 1414–1418, https://doi.org/10.1002/ange.201306559.
[18] F. Liu, E.B. Pak, B. Singh, C.M. Jensen, A.S. Goldman, Dehydrogenation of n-alkanes catalyzed by iridium "Pincer" complexes: regioselective formation of α-olefins, J. Am. Chem. Soc. 121 (1999) 4086–4087, https://doi.org/10.1021/ja983460p.
[19] J.-M. Basset, R. Psaro, D. Roberto, R. Ugo, Modern Surface Organometallic Chemistry, Wiley, 2009.
[20] M. Rimoldi, D. Fodor, J.A. van Bokhoven, A. Mezzetti, Catalytic hydrogenation of liquid alkenes with a silica-grafted hydride pincer iridium(iii) complex: support for a heterogeneous mechanism, Catal. Sci. Technol. 5 (2015) 4575–4586, https://doi.org/10.1039/C5CY00837A.
[21] C. Megías-Sayago, S. Ivanova, C. López-Cartes, M.A. Centeno, J.A. Odriozola, Gold catalysts screening in base-free aerobic oxidation of glucose to gluconic acid, Catal. Today 279 (2017) 148–154, https://doi.org/10.1016/j.cattod.2016.06.046.
[22] C. Megías-Sayago, K. Chakarova, A. Penkova, A. Lolli, S. Ivanova, S. Albonetti, F. Cavani, J.A. Odriozola, Understanding the role of the acid sites in 5-hydroxy-methylfurfural oxidation to 2,5-furandicarboxylic acid reaction over gold catalysts: surface investigation on CexZr1- xO2 compounds, ACS Catal. 8 (2018) 11154–11164, https://doi.org/10.1021/acscatal.8b02522.
[23] C. Megías-Sayago, J.M. Martínez Blanes, B.M. Szyja, J.A. Odriozola, S. Ivanova, How a small modification in the imidazolium-based SDA can determine the zeolite structure? MFI vs. TON, Microporous Mesoporous Mater. 322 (2021), 111160, https://doi.org/10.1016/j.micromeso.2021.111160.
[24] F. Ocampo, H.S. Yun, M.M. Pereira, J.P. Tessonnier, B. Louis, Design of MFI zeolite-based composites with hierarchical pore structure: a new generation of structured catalysts, Cryst. Growth Des. 9 (2009) 3721–3729, https://doi.org/10.1021/cg900425r.
[25] J. Okal, L. Kępiński, L. Krajczyk, M. Drozd, Oxidation and redispersion of a Re/γ-Al2O3 catalyst, J. Catal. 188 (1999) 140–153, https://doi.org/10.1006/jcat.1999.2634.
[26] Y. Maksimov, Structural investigation of Re2O7/Al2O3 catalysts for olefin disproportionation, J. Catal. 45 (1976) 114–117, https://doi.org/10.1016/0021-9517(76)90062-2.
[27] S. Vorakitkanvasin, S.K.N. Ayudhya, K. Suriye, P. Praserthdam, J. Panpranot, Enhanced metathesis activity of low loading Re2O7/Al2O3 catalysts for propylene production by using aluminum nitrate as Al2O3 precursor, Appl. Catal. A Gen. 517 (2016) 39–46, https://doi.org/10.1016/j.apcata.2016.01.008.
[28] J.A. Moulijn, J.C. Mol, Structure and activity of rhenium-based metathesis catalysts, J. Mol. Catal. 46 (1988) 1–14, https://doi.org/10.1016/0304-5102(88)85080-6.
[29] A.A. Tsyganenko, P.P. Mardilovich, Structure of alumina surfaces, Journal of the Chemical Society, Faraday Trans. 92 (1996) 4843, https://doi.org/10.1039/ft9969204843.
[30] C. Morterra, G. Magnacca, A case study: surface chemistry and surface structure of catalytic aluminas, as studied by vibrational spectroscopy of adsorbed species, Catal. Today 27 (1996) 497–532, https://doi.org/10.1016/0920-5861(95)00163-8.
[31] W. El-Nadjar, M. Bonne, E. Trela, L. Rouleau, A. Mino, S. Hocine, E. Payen, C. Lancelot, C. Lamonier, P. Blanchard, X. Courtois, F. Can, D. Duprez, S. Royer, Infrared investigation on surface properties of alumina obtained using recent templating routes, Microporous Mesoporous Mater. 158 (2012) 88–98, https://doi.org/10.1016/j.micromeso.2012.03.006.
[32] M. DIGNE, P. SAUTET, P. RAYBAUD, P. EUZEN, H. TOULHOAT, Hydroxyl groups on γ-alumina surfaces: a DFT study, J. Catal. 211 (2002) 1–5, https://doi.org/10.1006/jcat.2002.3741.
[33] H. Knözinger, P. Ratnasamy, Catalytic aluminas: surface models and characterization of surface sites, Catal. Rev. 17 (1978) 31–70, https://doi.org/10.1080/03602457808080878.
[34] C. Copéret, A. Comas-Vives, M.P. Conley, D.P. Estes, A. Fedorov, V. Mougel, H. Nagae, F. Núñez-Zarur, P.A. Zhizhko, Surface organometallic and coordination chemistry toward single-site heterogeneous catalysts: strategies, methods, structures, and activities, Chem. Rev. 116 (2016) 323–421, https://doi.org/10.1021/acs.chemrev.5b00373.
[35] Z.-W. Peng, P.-T. Hsieh, Y.-J. Lin, C.-J. Huang, C.-C. Li, Investigation on blistering behavior for n-type silicon solar cells, Energy Procedia 77 (2015) 827–831, https://doi.org/10.1016/j.egypro.2015.07.117.
[36] C. Liu, Q. Ma, H. He, G. He, J. Ma, Y. Liu, Y. Wu, Structure–activity relationship of surface hydroxyl groups during NO2 adsorption and transformation on TiO2 nanoparticles, Environ. Sci. Nano 4 (2017) 2388–2394, https://doi.org/10.1039/C7EN00920H.
[37] W. al Maksoud, L.E. Gevers, J. Vittenet, S. Ould-Chikh, S. Telalovic, K. Bhatte, E. Abou-Hamad, D.H. Anjum, M.N. Hedhili, V. Vishwanath, A. Alhazmi, K. Almusaiteer, J.M. Basset, A strategy to convert propane to aromatics (BTX) using TiNp4 grafted at the periphery of ZSM-5 by surface organometallic chemistry, Dalton Trans. 48 (2019) 6611–6620, https://doi.org/10.1039/C9DT00905A.
[38] E. Loeffler, U. Lohse, C. Peuker, G. Oehlmann, L.M. Kustov, V.L. Zholobenko, V. B. Kazansky, Study of different states of nonframework aluminum in hydrothermally dealuminated HZSM-5 zeolites using diffuse reflectance i.r. spectroscopy, Zeolites 10 (1990) 266–271, https://doi.org/10.1016/0144-2449(94)90138-4.
[39] H. Zhou, W. Zhu, L. Shi, H. Liu, S. Liu, Y. Ni, Y. Liu, Y. He, S. Xu, L. Li, Z. Liu, In situ DRIFT study of dimethyl ether carbonylation to methyl acetate on H-mordenite, J. Mol. Catal. A Chem. 417 (2016) 1–9, https://doi.org/10.1016/j.molcata.2016.02.032.
[40] B.C. Vicente, Z. Huang, M. Brookhart, A.S. Goldman, S.L. Scott, Reactions of phosphinites with oxide surfaces: a new method for anchoring organic and organometallic complexes, Dalton Trans. 40 (2011) 4268, https://doi.org/10.1039/c0dt01369b.
[41] M. Rimoldi, A. Mezzetti, Silica-grafted 16-electron hydride pincer complexes of iridium(III) and their soluble analogues: synthesis and reactivity with CO, Inorg. Chem. 53 (2014) 11974–11984, https://doi.org/10.1021/ic501593k.
[42] M. Liu, J.K. Zhuo, S.J. Xiong, Q. Yao, Catalytic degradation of high-density polyethylene over a clay catalyst compared with other catalysts, Energy Fuels 28 (2014) 6038–6045, https://doi.org/10.1021/ef501326k.
[43] A.A. Ajibola, J.A. Omoleye, V.E. Efeovbokhan, Catalytic cracking of polyethylene plastic waste using synthesised zeolite Y from Nigerian kaolin deposit, Appl. Petrochem Res. 8 (2018) 211–217, https://doi.org/10.1007/s13203-018-0216-7.
[44] S. Wu, X. Yang, C. Janiak, Confinement effects in zeolite-confined noble metals, Angew. Chem. 131 (2019) 12468–12482, https://doi.org/10.1002/ange.201900013.
[45] M. Marczewski, A. Jakubiak, H. Marczewska, A. Frydrych, M. Gontarz, A. Śnieguła, Acidity of sulfated oxides: Al2O3, TiO2 and SiO2. Application of test reactions, Phys. Chem. Chem. Phys. 6 (2004) 2513–2522, https://doi.org/10.1039/B400625A.
[46] J. Aguado, D.P. Serrano, J.M. Escola, A. Peral, Catalytic cracking of polyethylene over zeolite mordenite with enhanced textural properties, J. Anal. Appl. Pyrolysis 85 (2009) 352–358, https://doi.org/10.1016/j.jaap.2008.10.009.